Intercalation of L-Dopa into Layered Double Hydroxides: Enhancement of Both Chemical and Stereochemical Stabilities of a Drug through Host−Guest Interactions

Min Wei,* Min Pu, Jian Guo, Jingbin Han, Feng Li, Jing He, David G. Evans, and Xue Duan

State Key Laboratory of Chemical Resource Engineering, Beijing University of Chemical Technology, Beijing 100029, China

This paper describes a systematic study on the intercalation of an unstable chiral drug L-dopa into layered double hydroxides (LDHs) and the enhancement of its chemical and stereochemical stabilities through host−guest interactions, by virtue of combining experimental and theoretical investigations. L-Dopa has been intercalated into a magnesium−aluminum LDH, and the structural characterization reveals that L-dopa anions are accommodated vertically in the interlayer region as a monolayer of partially superimposed species. Thermogravimetry−mass spectroscopy and polarimetry indicate that both the chemical and stereochemical stabilities of L-dopa are enhanced significantly in a confined region between LDH sheets compared with pristine L-dopa. The racemization phenomenon of pristine L-dopa has been rationalized by quantum mechanical calculations at the B3PW91/6-31G(d,p) level. The computed results suggest that in the solid state L-dopa undergoes racemization via an enol intermediate formed by hydrogen transfer from the chiral carbon atom to the carboxylate group. After intercalation in the interlayer galleries of the LDH, the carboxylate group of the L-dopa becomes involved in strong host−guest interactions with the layers, with the computed binding energy of L-dopa to the LDH layers being ca. −1100 kJ/mol. The host−guest interactions, including electrostatic and hydrogen bonding between L-dopa and LDH host, thus inhibit the racemization reaction of the guest because the carboxylate group is no longer able to act as a hydrogen acceptor. Therefore, the results of theoretical study are in good agreement with those of the experimental ones. The results show that these layered materials have potential applications as the basis of a novel storage and delivery system for L-dopa or other unstable chiral pharmaceutical agents.

1. Introduction

Layered double hydroxides (LDHs), also known as hydrotalcite-like compounds, have received increasing attention as host materials for the construction of host−guest supramolecular structures. LDHs, which can be represented by the general formula $[M^{II}_{1−x}M^{III}_x(OH)_2]^{x+}(A^{n−})_{x/n} \cdot mH_2O$, are layered solids having positively charged layers and charge-compensating interlayer anions,[1] where M^{II} and M^{III} are di- and trivalent metals, respectively;[2] the coefficient x generally ranges between 0.20 and 0.33,[3] and $A^{n−}$ is an exchangeable inorganic (e.g., carbonate, nitrate, chloride, anionic coordina-

tion compounds, etc.),[4,5] organic (e.g., anionic polymers,[6,7] biological molecules,[8–12] anionic drugs,[13,14] etc.), or other anions (e.g., heteropolyacids, etc.).[15–17] The structure of LDHs is related to that of brucite, where the cations occupy the centers of octahedra which can form two-dimensional infinite sheets by sharing their edges and the hydroxyl group is located on the vertices of the octahedra with its hydrogen

* Corresponding author. Tel.: +86-10-64412131. Fax: +86-10-64425385. E-mail: weimin@mail.buct.edu.cn.

(1) (a) Braterman, P. S.; Xu, Z. P.; Yarberry, F. *Handbook of Layered Materials*; Marcel Dekker: New York, 2004; Chapter 8, p 373. (b) Evans, D. G.; Duan, X. *Chem. Commun.* **2006,** 485. (c) Williams, G. R.; O'Hare, D. *J. Mater. Chem.* **2006,** *16,* 3065. (d) He, J.; Wei, M.; Li, B.; Kang, Y.; Evans, D. G.; Duan, X. *Struct. Bonding (Berlin)* **2006,** *119,* 89.

(2) (a) Cavani, F.; Trifirò, F.; Vaccari, A. *Catal. Today* **1991,** *11,* 173. (b) Allmann, R. *Acta. Crystallogr., Sect. B* **1968,** *24,* 972. (c) Prevot, V.; Forano, C.; Besse, J. P. *Chem. Mater.* **2005,** *17,* 6695.

(3) (a) Ma, R. Z.; Liu, Z. P.; Takada, K.; Iyi, N.; Bando, Y.; Sasaki, T. *J. Am. Chem. Soc.* **2007,** *129,* 5257. (b) Khan, A. I.; O'Hare, D. *J. Mater. Chem.* **2002,** *12,* 3191. (c) Radha, A. V.; Kamath, P. V.; Ravishankar, N.; Shivakumara, C. *Langmuir* **2007,** *23,* 7700.

(4) (a) Hou, X. Q.; Kalinichev, A. G.; Kirkpatrick, R. J. *Chem. Mater.* **2002,** *14,* 2078. (b) Radha, A. V.; Kamath, P. V.; Shivakumara, C. *J. Phys. Chem. B* **2007,** *111,* 3411. (c) Gago, S.; Pillinger, M.; Sá Ferreira, R. A.; Carlos, L. D.; Santos, T. M.; Gonçalves, I. S. *Chem. Mater.* **2005,** *17,* 5803.

(5) (a) Lee, J. H.; Rhee, S. W.; Jung, D. Y. *J. Am. Chem. Soc.* **2007,** *129,* 3522. (b) Xu, Z. P.; Braterman, P. S.; Yu, K.; Xu, H. F.; Wang, Y. F.; Brinker, C. J. *Chem. Mater.* **2004,** *16,* 2750.

(6) (a) Leroux, F.; Besse, J. P. *Chem. Mater.* **2001,** *13,* 3507. (b) Moujahid, E. M.; Dubois, M.; Besse, J. P.; Leroux, F. *Chem. Mater.* **2002,** *14,* 3799. (c) Darder, M.; López-Blanco, M.; Aranda, P.; Leroux, F.; Ruiz-Hitzky, E. *Chem. Mater.* **2005,** *17,* 1969.

(7) (a) Itoh, T.; Shichi, T.; Yui, T.; Takahashi, H.; Inui, Y.; Takagi, K. *J. Phys. Chem. B* **2005,** *109,* 3199. (b) Leroux, F.; Besse, J. P. *Chem. Mater.* **2001,** *13,* 3507. (c) Xiong, Z. G.; Xu, Y. M. *Chem. Mater.* **2007,** *19,* 1452. (d) Ding, P.; Zhang, M.; Gai, J.; Qu, B. J. *J. Mater. Chem.* **2007,** *17,* 1117.

(8) (a) Wei, M.; Yuan, Q.; Evans, D. G.; Wang, Z. Q.; Duan, X. *J. Mater. Chem.* **2005,** *15,* 1197. (b) Whilton, N. T.; Vickers, P. J.; Mann, S. *J. Mater. Chem.* **1997,** *7,* 1623.

(9) (a) Tamura, H.; Chiba, J.; Ito, M.; Takeda, T.; Kikkawa, S. *Solid State Ionics* **2004,** *172,* 607. (b) Nakayama, H.; Wada, N.; Tsuhako, M. *Int. J. Pharm.* **2004,** *269,* 469.

atom pointing toward the interlayer region.[15b] In LDHs, a fraction of the divalent cations in the brucite-like layers have been replaced isomorphously with trivalent cations,[10,18,19] which results in positively charged layers and the consequent intercalation of various anionic species into the interlayer region in order to maintain charge balance.

Many studies of new host−guest hybrid materials based on LDHs prepared by coprecipitation, ion exchange,[20] or calcination−rehydration[1] have highlighted their extensive applications as flame retardants,[16a,21] catalysts and catalyst precursors,[16b,22] adsorbents,[23] electrical and optical functional materials,[24] and materials for separation of organic isomers.[25,26] In the case of the pharmaceutical field, drug−LDH hybrids

have been synthesized and used as the basis of a controlled drug release system.[27] Early studies found that Mg/Al-LDHs can act as an ingredient in sustained-release pharmaceuticals containing nifedipine, for stabilizing pharmaceutical compositions and for preparing aluminum/magnesium salts of antipyretic, analgesic and anti-inflammatory drugs.[28] In recent years, in order to demonstrate the feasibility of LDH-based tunable drug delivery systems, a series of pharmaceutically active compounds, such as ibuprofen, diclofenac, gemfibrozil, naproxen, 2-propylpentanoic acid, 4-biphenylacetic acid, tolfenamic acid, indomethacin, and fenbufen, etc., have been intercalated into LDHs.[27a,29]

In general, most pharmaceutical agents are chiral,[30a] and some of their optical activity is readily lost by racemization under relatively mild conditions.[30] As a rule, while the one enantiomer has the desired therapeutic effect the other has none, at best, or is even deleterious.[30a] Therefore, the current general policy is to promote the commercialization of new chiral drugs marketed as single enantiomers wherever possible in order to reduce the required dose or avoid secondary effects. In order to maintain the efficacy of drugs which racemize under relatively mild conditions and ensure that the correct dose is administered, it is therefore necessary to find ways of inhibiting the rate of racemization.[30b–d]

In our previous work, we have reported the intercalation of the amino acid L-tyrosine into LDHs and shown that its thermal and chiral stability are increased after intercalation.[8a] L-Dopa, 3-(3,4-dihydroxyphenyl)-L-alanine [$(HO)_2C_6H_3$-$CH_2CH(NH_2)COOH$], is an effective precursor to several neurologically important catecholamines[31] and also is one of the major chiral pharmaceutical agents for the treatment of the main symptoms of Parkinson's disease.[32] Both the chemical and stereochemical stabilities of L-dopa are unstable, and its oxidation, decomposition, as well as racemization occur easily under mild conditions. Moreover, the enantiomer D-dopa has toxic properties, and use of racemic mixtures containing both L-dopa and D-dopa may cause serious side effects.[33] How to conserve L-dopa without racemization therefore, deserves much attention.

In this work, we have studied the intercalation of L-dopa into Mg/Al-LDH for the first time, in order to investigate the ability of the LDHs to act as a "molecular container" for L-dopa, and hence enhance its chemical and stereochemical stabilities. Recently, with the rapid development of

(10) Yuan, Q.; Wei, M.; Evans, D. G.; Duan, X. *J. Phys. Chem. B* **2004**, *108*, 12381.
(11) (a) Reinholdt, M. X.; Kirkpatrick, R. J. *Chem. Mater.* **2006**, *18*, 2567. (b) Darder, M.; López-Blanco, M.; Aranda, P.; Leroux, F.; Ruiz-Hitzky, E. *Chem. Mater.* **2005**, *17*, 1969.
(12) Desigaux, L.; Belkacem, M. B.; Richard, P.; Cellier, J.; Leone, P.; Cario, L.; Leroux, F.; Taviot-Gueho, C.; Pitard, B. *Nano Lett.* **2006**, *6*, 199.
(13) Mohanambe, L.; Vasudevan, S. *J. Phys. Chem. B* **2005**, *109*, 15651.
(14) (a) Gordijo, C. R.; Barbosa, C. A. S.; Ferreira, A. M.; Constantino, V. R. L.; Silva, D. *J. Pharm. Sci.* **2005**, *94*, 1135. (b) Dupina, J. C.; Martineza, H.; Guimona, C.; Dumitriub, E.; Fechete, I. *Appl. Clay Sci.* **2004**, *27*, 95. (c) Arcoa, M.; Sonia, G.; Cristina, M.; Vicente, R.; Joao, R. *J. Solid State Chem.* **2004**, *177*, 3954. (d) Zhang, H.; Zou, K.; Guo, S. H.; Duan, X. *J. Solid State Chem.* **2006**, *179*, 1791.
(15) (a) Weir, M. R.; Moore, J.; Kydd, R. A. *Chem. Mater.* **1997**, *9*, 1686. (b) Silva, L. F.; Tronto, J.; Oliveira, H. P.; Valim, J. B. *J. Inclusion Phenom. Macrocyclic Chem.* **2003**, *46*, 187. (c) Frunza, L.; Scho1nhals, A.; Frunza, S.; Parvulescu, V. I.; Cojocaru, B.; Carriazo, D.; Martın, C.; Rives, V. *J. Phys. Chem. A* **2007**, *111*, 5166. (d) Sels, B. F.; De Vos, D. E.; Jacobs, P. A. *J. Am. Chem. Soc.* **2007**, *129*, 6916.
(16) (a) Williams, G. R.; Norquist, A. J.; O'Hare, D. *Chem. Mater.* **2004**, *16*, 975. (b) Villegas, J. C.; Giraldo, O. H.; Laubernds, K.; Suib, S. L. *Inorg. Chem.* **2003**, *42*, 5621. (c) Arco, M.; Carriazo, D.; Gutiérrez, S.; Martı́n, C.; Rives, V. *Inorg. Chem.* **2004**, *43*, 375.
(17) (a) Cervilla, A.; Corma, A.; Fornbs, V.; Llopis, E.; Palanca, P.; Rey, F.; Riberat, A. *J. Am. Chem. Soc.* **1994**, *116*, 1595. (b) Venugopal, B. R.; Ravishankar, N.; Perrey, C. R.; Shivakumara, C.; Rajamathi, M. *J. Phys. Chem. B* **2006**, *110*, 772. (c) Gardner, E.; Huntoon, K. M.; Pinnavaia, T. J. *Adv. Mater.* **2001**, *13*, 1263.
(18) Xu, Z. P.; Stevenson, G. S.; Lu, C. Q.; Lu, G. Q.; Bartlett, P. F.; Gray, P. P. *J. Am. Chem. Soc.* **2006**, *128*, 36.
(19) Newman, S. P.; Williams, S. J.; Coveney, P. V.; Jones, W. *J. Phys. Chem. B* **1998**, *102*, 6710.
(20) Crepaldi, E. L.; Pavan, P. C.; Valim, J. B. *Chem. Commun.* **1999**, 155.
(21) (a) Wang, Z. Y.; Han, E. H.; Ke, W. *Prog. Org. Coat.* **2005**, *53*, 29. (b) Costache, M. C.; Wang, D. Y.; Heidecker, M. J.; Manias, E.; Wilkie, C. A. *Polym. Adv. Technol.* **2006**, *17*, 272. (c) Gursky, J. A.; Blough, S. D.; Luna, C.; Gomez, C.; Luevano, A. N.; Gardner, E. A. *J. Am. Chem. Soc.* **2006**, *128*, 8376.
(22) (a) Kagunya, W.; Hassan, Z.; Jones, W. *Inorg. Chem.* **1996**, *35*, 5970. (b) Choudary, B. M.; Madhi, S.; Chowdari, N. S.; Kantam, M. L.; Sreedhar, B. *J. Am. Chem. Soc.* **2002**, *124*, 14127. (c) Sels, B. F.; De Vos, D. E.; Grobet, P. J.; Pierard, F.; Mesmaeker, F. K. D.; Jacobs, P. A. *J. Phys. Chem. B* **1999**, *103*, 11114. (d) Greenwell, H. C.; Stackhouse, S.; Coveney, P. V.; Jones, W. *J. Phys. Chem. B* **2003**, *107*, 3476. (e) Choudary, B. M.; Jaya, V. S.; Reddy, B. R.; Kantam, M. L.; Rao, M. M.; Madhavendra, S. S. *Chem. Mater.* **2005**, *17*, 2740.
(23) (a) Pavan, P. C.; Gomes, G. A.; Valim, J. B. *Microporous Mesoporous Mater.* **1998**, *21*, 659. (b) Dutta, P. K.; Robins, D. S. *Langmuir* **1994**, *10*, 1851. (c) Jiang, J. Q.; Xu, Y. L.; Quill, K.; Simon, J.; Shettle, K. *Ind. Eng. Chem. Res.* **2007**, *46*, 4577.
(24) (a) Katz, E.; Lioubashevski, O.; Willner, I. *J. Am. Chem. Soc.* **2005**, *127*, 3979. (b) Ogawa, M. *Chem. Rev.* **1995**, *95*, 399. (c) Lang, K.; Bezdicka, P.; Bourdelande, J. L.; Hernando, J.; Jirka, I.; Kafunkova, E.; Kovanda, F.; Kubat, P.; Mosinger, J.; Wagnerova, D. M. *Chem. Mater.* **2007**, *19*, 3822. (d) Chen, H. Y.; Zhang, F. Z.; Fu, S. S.; Duan, X. *Adv. Mater.* **2006**, *18*, 3089.
(25) Fogg, A. M.; Green, V. M.; Harvey, H. G.; O'Hare, D. *Adv. Mater.* **1999**, *11*, 1466.
(26) (a) Millange, F.; Walton, R. I.; Lei, L.; O'Hare, D. *Chem. Mater.* **2000**, *12*, 1990. (b) Ragavan, A.; Khan, A. I.; O'Hare, D. *J. Mater. Chem.* **2006**, *16*, 602.
(27) (a) Khan, A. I.; Lei, L.; Norquist, A. J.; O'Hare, D. *Chem. Commun.* **2001**, 2342. (b) Xu, Z. P.; Zeng, Q. H.; Lua, G. Q.; Yu, A. B. *Chem. Eng. Sci.* **2006**, *61*, 1027. (c) Li, L.; Ma, R. Z.; Iyi, N.; Ebina, Y.; Takada, K.; Sasaki, T. *Chem. Commun.* **2006**, 3125.
(28) (a) Yang, J. H.; Han, Y. S.; Park, M.; Park, T.; Hwang, S. J.; Choy, J. H. *Chem. Mater.* **2007**, *19*, 2679. (b) Ambrogi, V.; Fardella, G.; Grandolini, G.; Perioli, L. *Int. J. Pharm.* **2001**, *220*, 23.
(29) (a) Wei, M.; Shi, S. X.; Wang, J.; Li, Y.; Duan, X. *J. Solid State Chem.* **2004**, *177*, 2534. (b) Arco, M. D.; Cebadera, E.; Gutiérrez, S.; Martén, C.; Montero, M. J.; Rives, V.; Rocha, J.; Sevilla, M. A. *J. Pharm. Sci.* **2004**, *93*, 1649.
(30) (a) Patel, R. N.; Hanson, R. L.; Banerjee, A.; Szarka, L. J. *J. Am. Oil Chem. Soc.* **1997**, *74*, 1345. (b) Reist, M.; Testa, B.; Carrupt, P. A.; Jung, M.; Schuring, V. *Chirality* **1995**, *7*, 396. (c) Wsol, V.; Skalova, L.; Szotakova, B. *Curr. Drug Metab.* **2004**, *5*, 517. (d) Shinitzky, M.; Nudelman, F.; Barda, Y.; Haimovitz, R.; Chen, E.; Deamer, D. W. *Origins Life Evol. Biosphere* **2002**, *32*, 285.
(31) Pattison, D. I.; Dean, R. T.; Davies, M. J. *Toxicology* **2002**, *177*, 23.
(32) Lai, C. T.; Yu, P. H. *Biochem. Pharmacol.* **1997**, *53*, 363.
(33) Shen, J. S.; Zhao, S. L. *J. Chromatogr.* **2004**, *1059*, 209.

computer power, the use of computational methods for the study of the microstructure of LDHs has become a useful adjunct to experimental techniques. We have employed density functional theory (DFT) theoretical computations to probe the mechanism of racemization of L-dopa and the effect of the LDH host on the rate of racemization. It was found that the results of theoretical study are in accordance with those of the experimental ones, demonstrating the influence of host−guest interactions on the stability of the intercalated guest. Our aim is to use a combination of experimental measurements and theoretical computations in order to understand how the host inhibits racemization of L-dopa and, hence, facilitate the formulation of materials that have potential applications as the basis of a novel storage and delivery system for L-dopa or other unstable chiral pharmaceutical molecules.

2. Experimental Section

2.1. Materials. L-Dopa was purchased from Sigma, and other inorganic chemicals including $Mg(NO_3)_2 \cdot 6H_2O$, $Al(NO_3)_3 \cdot 9H_2O$, NaOH, etc., were of analytical grade and used without further purification.

2.2. Preparation of L-Dopa−Mg/Al-LDH. The precursor, an LDH in the nitrate form, was synthesized by a procedure similar to that reported previously.[13] A solution of magnesium and aluminum nitrates (molar ratio 2:1) in deionized water was added dropwise to a solution of sodium hydroxide with vigorous agitation under a nitrogen atmosphere. The mixture was aged at 70 °C for 40 h after the solution pH was adjusted to 10.0. The resulting white precipitate was separated by centrifugation, washed thoroughly with deionized water, and dried at 70 °C for 18 h.

The L-dopa−Mg/Al-LDH was prepared via two successive ion-exchange processes. The $LDH-NO_3$ precursor (8.3 g, ca. 2 mmol) was added to a solution of L-dopa (0.79 g, ca. 4 mmol) in deionized water with vigorous agitation under a nitrogen atmosphere, avoiding sunlight. The mixture (ca. pH 7.7) was kept for 48 h at 20 °C. The precipitate was washed and centrifuged three times. In order to maximize the extent of intercalation of L-dopa in the LDH, a second ion-exchange process using the precipitate obtained was performed under the same conditions to those described above. Finally, the resulting product was dried in a vacuum desiccator at room temperature. Elemental analysis: found (calcd for $Mg_{2.06}Al$-$(OH)_{6.12}(C_9H_{11}NO_4)_{0.60}(CO_3)_{0.20} \cdot 1.73H_2O$) Mg 14.37% (14.46%), Al 6.98% (7.89%), C 19.40% (19.66%), N 1.98% (2.46%), H 4.25% (4.73%).

2.3. Characterization. Powder X-ray diffraction (XRD) measurements were performed on a Rigaku D/MAX2500VB2+/PC diffractometer, using Cu Kα radiation ($\lambda = 0.154$ nm) at 40 kV, 200 mA, a scanning rate of 5°/min, and a 2θ angle ranging from 3° to 70°. Fourier transform infrared (FT-IR) spectra were recorded using a Vector 22 (Bruker) spectrophotometer in the range of $4000-400$ cm^{-1} with 2 cm^{-1} resolution. The standard KBr disk method (1 mg of sample in 100 mg of KBr) was used. UV−vis spectra were recorded on a Shimadzu UV-2501PC spectrometer in the wavelength range of $200-700$ nm after dissolution of samples in HCl solution (1:1, v/v), and quantitative analysis was performed at 280.0 nm. Microanalysis of metals was performed by inductively coupled plasma (ICP) emission spectroscopy on a Shimadzu ICPS-7500 instrument using solutions prepared by dissolving samples in dilute HNO_3. Carbon, hydrogen, and nitrogen analyses were carried out using an Elementarvario elemental analysis instrument. Thermogravimetric/differential thermal analysis (TG/DTA) traces were measured on a PCT-1A thermal analysis system in air with a heating rate of 10 °C/min. Thermogravimetry−mass spectrometry (TG−MS) measurements were carried out on a Pyris Diamond TG instrument equipped with a mass spectrometer (ThermoStar TM) in an inert atmosphere (N_2). The temperature-programmed ramp rate was 10 °C/min, and the temperature ranges from 30 to 700 °C. Gaseous emission was analyzed at intervals of 1 s. Solid-state ^{13}C nuclear magnetic resonance (NMR) spectra were run on a Bruker AV600 spectrometer operating at a frequency of 150.9430 MHz for ^{13}C with a 3 s pulse delay. Optical rotation measurements were carried out on a WZZ-1S automatic polarimeter at 589.3 nm (Na D-line).

2.4. Study of the Racemization of L-Dopa. Investigations of the racemization of pristine L-dopa and L-dopa−LDH were performed under three different conditions: (1) exposure to sunlight for different times; (2) irradiation by UV light (Hg lamp) for various times; (3) heat treatment at 20, 50, 80, 120, 160, and 200 °C for 1 h. Subsequently, each sample was dissolved using 20 mL of 1 mol·L^{-1} HCl and the optical rotation was measured at room temperature (about 18 °C) using a polarimeter with a 10 cm sample tube. It should be noted that the ionic strength and pH of the pristine L-dopa solution were adjusted to the same values as those of the L-dopa−LDH solution before measurement.
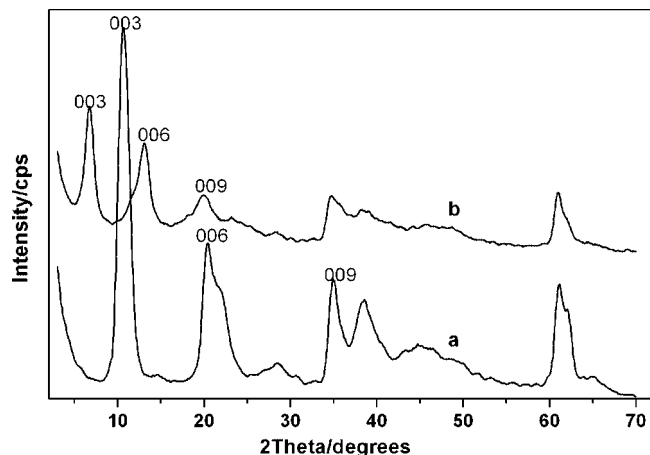
2.5. In Vitro Drug Release. A multipoint working curve was made. A series of solutions in simulated intestinal fluids (phosphate buffers with pH 7.6 and 6.4) with the concentration of L-dopa in the range of $0-100$ ppm were prepared. The UV absorbance of the solution at 280.0 nm was plotted versus the concentration of L-dopa, and thus linear equations were obtained for the different pH values: concn $= 0.01417A + 0.00385$, where $R = 0.99987$ (pH 7.6); concn $= 0.01483A - 0.00279$, where $R = 0.99992$ (pH 6.4).

Drug release tests were carried out at constant temperature (37 ± 0.5 °C) by suspending L-dopa−Mg/Al-LDH (0.15 g) in phosphate buffer (150 mL). Aliquots (2 mL) of the supernatant were removed at intervals and diluted to 20 mL with the corresponding buffer solution, and the L-dopa content was determined by UV absorbance at 280.0 nm. In order to determine the amount of drug corresponding to total release, Na_2CO_3 (0.53 g) was dissolved in a suspension with the above composition and the mixture was stirred for 2 h (carbonate has a strong affinity for LDHs and can be expected[1] to replace all of the L-dopa in L-dopa−Mg/Al-LDH by ion exchange), and the concentration of L-dopa was also determined by the method described above.

3. Theoretical Computations

In order to give a detailed understanding of how the host−guest interactions influence the stereochemical stability of the guest, the racemization phenomenon of pristine L-dopa has been rationalized by quantum mechanical calculations at the B3PW91/6-31G(d,p) level. The geometries of the reactant, product, intermediate, and transition states for the racemization reaction of L-dopa molecules were fully optimized by using DFT at the B3PW91/6-31G(d,p) level. The vibrational analysis of all the species were calculated in order to verify the nature of the equilibrium and transition states, and the zero-point energy (ZPE) was also obtained at the same time. The single-point energies of the equilibrium state and transition state on the excited state (S_1, T_1) were computed by using time-dependent density functional theory (TDDFT). The Gaussian 03 program package[34] was used in
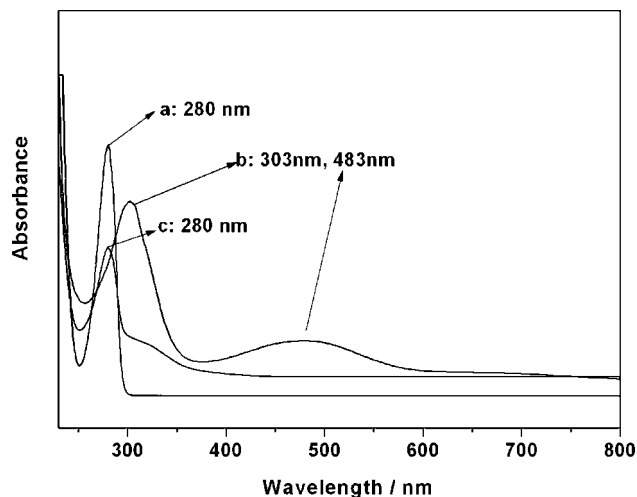
Figure 1. Powder XRD patterns of (a) NO$_3$−Mg/Al-LDH and (b) L-dopa−Mg/Al-LDH.

Figure 2. UV−vis spectra of (a) pristine L-dopa, (b) the oxidation product of L-dopa in air, and (c) L-dopa−LDH.

all the quantum chemical calculations. The molecular structural models were drawn using the Alchemy software.

4. Results and Discussion

4.1. Characterization of L-Dopa−Mg/Al-LDH. *4.1.1. X-ray Diffraction.* The powder XRD patterns of the NO$_3$−Mg/Al-LDH precursor and the product of its reaction with L-dopa in two successive exchange reactions (2 days + 2 days) carried out at room temperature under nitrogen in the absence of sunlight at pH 7.7 are shown in Figure 1. In each case, the reflections can be indexed to a single phase with $R\bar{3}m$ rhombohedral symmetry, commonly used for the description of the LDH structures.[10,35] In comparison with the precursor, the (00*l*) reflections of the product moved to lower 2θ angle, i.e., from 10.71° to 6.73° (003) and from 20.45° to 13.00° (006). This corresponds to an increase in interlayer distance (d_{003}) from 0.825 to 1.312 nm, which is indicative of the intercalation of L-dopa into the interlayer galleries of the LDH by anion exchange with NO$_3$⁻. The (110) reflection at about 60° showed no obvious shift after intercalation, indicating that no significant change occurred in the LDH host layers.[1]

4.1.2. Spectroscopic Studies. It has been reported that L-dopa is readily oxidized under moist alkaline conditions, forming a dark-colored compound.[36] Therefore, UV−vis, FT-IR, and ^{13}C NMR spectroscopy as well as polarimetry were

used to investigate whether intercalation of L-dopa into the LDH host was associated with any change in its chemical and/or stereochemical structure. Figure 2 shows the UV−vis spectra of pristine L-dopa (Figure 2a), the oxidation product of L-dopa in air (Figure 2b), and L-dopa−LDH (Figure 2c). It can be seen that pristine L-dopa exhibits a strong absorption band at 280 nm, whereas its oxidation product displays two bands at 303 and 483 nm. This is consistent with the results reported by Barreto et al.;[37] the band at 280 nm in pristine L-dopa is attributed to the phenolic structure, whereas the bands at 303 and 483 nm correspond to electronic transitions of the quinone form. After intercalation in the LDH host, no shift in the band at 280 nm was observed indicating that no significant oxidation of L-dopa occurred during the formation of L-dopa−LDH by ion exchange.

The FT-IR spectra of pristine L-dopa, L-dopa−LDH, and the NO$_3$−LDH precursor are shown in Figure 3. For the sake of clarity, only the main absorption bands were listed. In the spectrum of L-dopa (Figure 3a), the bands at 3375, 3209, and 3067 cm⁻¹ can be attributed to ν(N−H), ν(O−H), and ν(Ar−H) vibrations, respectively. The strong absorption bands at 1590 and 1404 cm⁻¹ are characteristic of the asymmetric and symmetric stretching vibrations of carboxyl group,[2b] respectively. The bands centered at 1676 and 1258

(34) Frisch, M. J.; Trucks, G. W.; Schlegel, H. B.; Scuseria, G. E.; Robb, M. A.; Cheeseman, J. R.; Montgomery, J. A., Jr.; Vreven, T.; Kudin, K. N.; Burant, J. C.; Millam, J. M.; Iyengar, S. S.; Tomasi, J. J.; Barone, V.; Mennucci, B.; Cossi, M.; Scalmani, G.; Rega, N.; Petersson, G. A.; Nakatsuji, H.; Hada, M.; Ehara, M.; Toyota, K.; Fukuda, R.; Hasegawa, J.; Ishida, M.; Nakajima, T.; Honda, Y.; Kitao, O.; Nakai, H.; Klene, M.; Li, X.; Knox, J. E.; Hratchian, H. P.; Cross, J. B.; Adamo, C.; Jaramillo, J.; Gomperts, R.; Stratmann, R. E.; Yazyev, O.; Austin, A. J.; Cammi, R.; Pomelli, C.; Ochterski, J. W.; Ayala, P. Y.; Morokuma, K.; Voth, A.; Salvador, P.; Dannenberg, J. J.; Zakrzewski, V. G.; Dapprich, S.; Daniels, A. D.; Strain, M. C.; Farkas, O.; Malick, D. K.; Rabuck, A. D.; Raghavachari, K.; Foresman, J. B.; Ortiz, J. V.; Cui, Q.; Baboul, A. G.; Clifford, S.; Cioslowski, J.; Stefanov, B. B.; Liu, G.; Liashenko, A.; Piskorz, P.; Komaromi, I.; Martin, R. L.; Fox, D. J.; Keith, T.; Al-Laham, M. A.; Peng, C. Y.; Nanayakkara, A.; Challacombe, M.; Gill, P. M. W.; Johnson, B.; Chen, W.; Wong, M. W.; Gonzalez, C.; Pople, J. A. *Gaussian 03*, revision B.04; Gaussian, Inc.: Pittsburgh, PA, 2003.
(35) Vaysse, C.; Guerlou-Demourgues, L.; Delmas, C. *Inorg. Chem.* **2002**, *41*, 6905.
(36) Findrik, Z.; Geueke, B.; Hummel, W.; Vası́c-Răcki, D. *Biochem. Eng. J.* **2006**, *27*, 275.
(37) Barreto, W. J.; Ponzoni, S.; Sassi, P. *Spectrochim. Acta, Part A* **1999**, *55*, 65.
(38) (a) Duff, G. A.; Roberts, J. E.; Foster, N. *Biochemistry* **1988**, *27*, 7112. (b) Challener, C. A. *Chiral Drugs*; Ashgate Publishing Ltd.: Hampshire, UK. 2004; p 339. (c) Challener, C. A. *Chiral Intermediates*; Ashgate Publishing Ltd.: Hampshire, UK. 2004; p 476.
(39) (a) Éhen, Zs.; Novák, Cs.; Sztatisz, J.; Bene, O. *J. Therm. Anal. Calorim.* **2004**, *78*, 427. (b) Perng, L. H. *J. Polym. Res.* **2000**, *7*, 185. (c) Surianarayanan, M.; Uchida, T.; Wakakura, M. *J. Loss Prev. Proc. Ind.* **1998**, *11*, 99.
(40) (a) Challener, C. A. *Chiral Drugs*; Ashgate Publishing Ltd.: Hampshire, UK. 2004; p 339. (b) Challener, C. A. *Chiral Intermediates*; Ashgate Publishing Ltd.: Hampshire, UK. 2004; p 476.
(41) (a) Orwa, J. A.; Govaerts, C.; Gevers, K.; Roets, E.; Van Schepdael, A.; Hoogmartens, J. *J. Pharm. Biomed. Anal.* **2002**, *29*, 203. (b) Guo, C.; Shah, R. D.; Mills, J.; Dukor, R. K.; Cao, X.; Freedman, T. B.; Nafie, L. A. *Chirality* **2006**, *18*, 775. (c) Matsuo, K.; Yamamoto, Y.; Kado, N.; Yamazaki, M.; Nagata, O.; Kato, H.; Tsuji, A. *Chem. Pharm. Bull.* **2001**, *49*, 794. (d) Vakily, M.; Corrigan, B.; Jamali, F. *Pharm. Res.* **1995**, *12*, 1652.
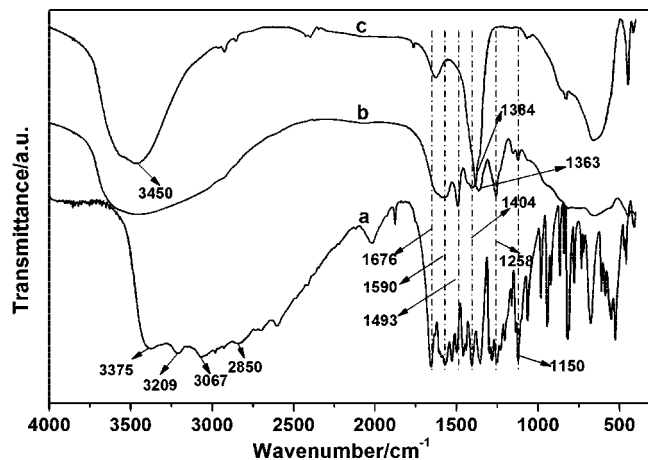
Figure 3. FT-IR spectra of (a) pristine L-dopa, (b) L-dopa−LDH, and (c) NO₃−LDH.

Figure 4. Solid-state ¹³C NMR spectra of (a) L-dopa and (b) L-dopa−LDH.

cm⁻¹ are assigned to C=C and C−N stretching vibrations, and those at 1493 and 1150 cm⁻¹ are due to δ(N−H) and δ(O−H) deformation modes, respectively. The other absorption bands below 1000 cm⁻¹ are attributed to δ(C−H) deformation modes. The spectrum of NO₃−LDH precursor (Figure 3c) shows a broad absorption band at 3450 cm⁻¹ due to the stretching vibration of the hydroxyl group in the LDH layers and interlayer water molecules. The band at 1384 cm⁻¹ is assigned to the stretching vibration of interlayer NO_3^-. The spectrum of L-dopa−LDH (Figure 3b) shows a very broad band (3700−3000 cm⁻¹) due to the stretching vibrations of the NH₂ group of L-dopa, the OH group of L-dopa, and interlayer water. Moreover, characteristic bands of L-dopa at 1590, 1493, 1404, 1258, and 1150 cm⁻¹ were observed. Meanwhile, the absorption band of interlayer NO_3^- at 1384 cm⁻¹ (Figure 3c) is absent in the spectrum of L-dopa−LDH (Figure 3b), confirming that the NO_3^- anion has been replaced by ion exchange. In addition, a band at 1363 cm⁻¹ is also observed which could be due to a small amount of CO_3^{2-} being cointercalated in the interlayer region; this is commonly observed[1] for exchange reactions of organic anions with LDHs, even when efforts are made to exclude atmospheric CO₂. The FT-IR spectra confirm that L-dopa has been successfully intercalated in the LDH host.

Supporting evidence for the intercalation of L-dopa in the LDH host was provided by solid-state ¹³C NMR spectroscopy. The solid-state ¹³C NMR spectrum of L-dopa (Figure 4a) displays resonances at 177.0 ppm C(1), 144.0 ppm C(8), 142.7 ppm C(7), 126.5 ppm C(4), 120.6 ppm C(6), 119.9 ppm C(9), 115.4 ppm C(5), 58.4 ppm C(2), and 37.9 ppm C(3). The other less intense features near the peaks of C(1) and C(2) are spinning sidebands.[38a] The ¹³C spectrum of L-dopa−LDH (Figure 4b) shows five broad bands. The broad resonances centered at 58 and 37 ppm result from aliphatic carbons C(2) and C(3). The broad resonance in the region 110−130 ppm can be ascribed to the nonhydroxyl-bearing carbon atoms [C(4), C(5), C(6), and C(9)] of the benzene ring. The resonances of C(7) and C(8) were shifted downfield by ca. 8 ppm upon intercalation, which may be attributed to the effect of hydrogen bonding between the hydroxyls and interlayer water molecules. In addition to the expected carboxyl C(1) resonance at ca. 175 ppm, a weak sharp
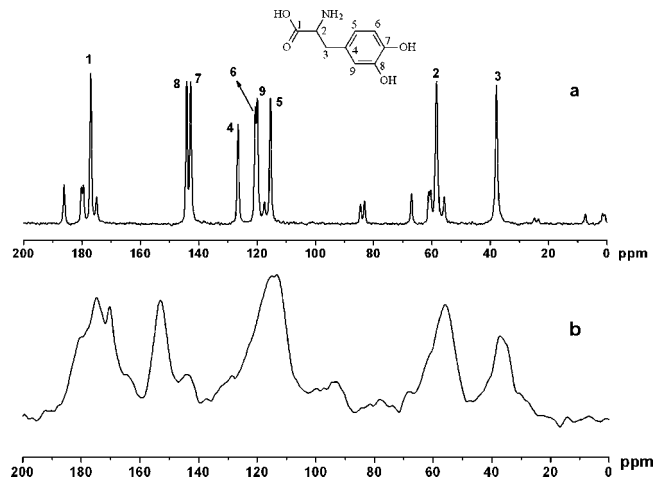
resonance was recorded at ca. 170 ppm, which is absent in the spectrum of pure L-dopa. This can be attributed to the cointercalation of a small amount of carbonate into the LDHs[8b,29b] and is consistent with the FT-IR data. The ¹³C NMR spectra therefore indicate that the integrity of the L-dopa molecule was preserved during intercalation, although the chemical environment of the interlayer L-dopa is somewhat different from that of the pristine form due to host−guest interactions.

4.1.3. Optical Activity of L-Dopa−LDH. Because of the unstable photochemical property and thus easy racemization of the chiral guest L-dopa, it is essential to determine whether L-dopa retains its stereochemical structure or not upon intercalation. In this work, the optical rotation of L-dopa before and after intercalation into the Mg/Al-LDH was measured, and thus the values of specific optical rotation of the materials are listed in Supporting Information Table S1. It can be seen that the experimental value of the specific optical rotation of fresh L-dopa ($\alpha_{589.3}^{18} = -11.8°$, 1 mol·L⁻¹ HCl) is close to the reported values,[38b,c] although little difference can be observed due to different measurement temperatures. In addition, the value of specific optical rotation for the intercalated L-dopa ($\alpha_{589.3}^{18} = -12.2°$, 1 N HCl) does not decrease compared with that of the pristine L-dopa, indicating that no racemization of L-dopa occurs during the intercalation process.

4.1.4. Chemical Composition and Structural Model. According to the elemental analysis data, the C/N ratio of the composite is 9.8, larger than that of pure L-dopa (9.0, based on the molecular formula C₉H₁₁NO₄). This is consistent with some CO_3^{2-} anions having also been intercalated into the interlayer region. The analytical data are consistent with the stoichiometry Mg₂.₀₆Al(OH)₆.₁₂(C₉H₁₁NO₄)₀.₆₀(CO₃)₀.₂₀· 1.73H₂O. The Mg²⁺/Al³⁺ molar ratio determined experimentally for the composite (2.06) is approximately equal to that in the synthesis mixture (2.00), and the content of intercalated L-dopa accounts for 75 mol % of the guest anions.

On the basis of the basal spacing d_{003} of 1.312 nm of L-dopa−LDH observed by XRD, and subtracting the thickness of the brucite layer (0.48 nm),[10] the gallery height is calculated to be 0.832 nm, very close to the length of the

Scheme 1. Possible Representation for the Structure of L-Dopa−LDH
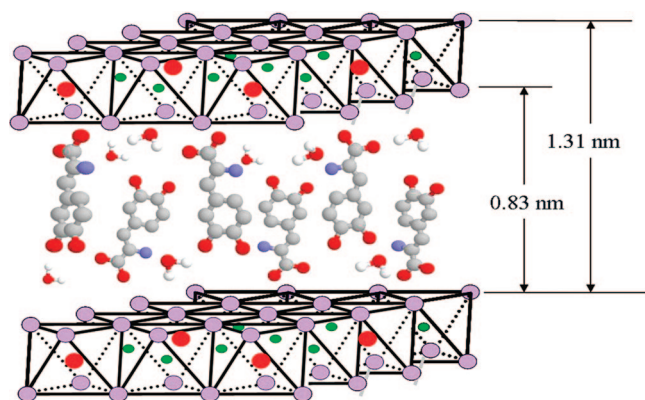
L-dopa anion (0.84 nm, calculated by the B3PW91/6-31G(d,p) level). By virtue of the presence of one carboxyl group, one amino group, and two hydroxyl groups in its structure, L-dopa shows a four-step dissociation in water solution, and Supporting Information Table S2 lists the values of pK_a and the distribution coefficient calculated according to the synthesis conditions with a solution pH 7.7 for the ion-exchange process. On this basis, it can be predicted that L-dopa exists mainly as a monovalent anion during the intercalation reaction. Therefore, we propose that L-dopa anions may be accommodated vertically in the interlayer region as a monolayer of partially superimposed species, with the carboxyl group of alternate anions attached to the upper or the lower hydroxide layers, as shown in Scheme 1. The interactions in the interlayer galleries consist of the electrostatic attraction between the positively charged host layers and negatively charged guests, as well as the hydrogen bonding formed between the host layers, the guest anions, and the interlayer water molecules.

4.2. Investigation of the Thermal Stability of L-Dopa−LDH. *4.2.1. Structural Changes with Increasing Temperature.* The variable temperature XRD patterns of the intercalation product recorded in the temperature range of 18−500 °C are shown in Figure 5A, and the variation in basal spacing d_{003} with temperature is given in Figure 5B. Heat treatment below 200 °C resulted in a gradual shift of the basal reflections to higher angle 2θ with increasing temperature (Figure 5A), and the value of the d_{003} basal spacing decreased from 1.45 nm at room temperature to 1.22 nm at 200 °C (Figure 5B). The observed contraction (0.23 nm) is very close to the calculated dimension of the hydrogen bonding space (0.22 nm) in LDHs,[8a] and therefore the decrease in d_{003} can be attributed to the loss of hydrogen bonding resulting from the deintercalation of interlayer water molecules. On raising the temperature from 200 to 300 °C, the (003) reflection moved to significantly higher angle 2θ, and its intensity significantly declined. The corresponding large contraction in d_{003} between 200 (1.22 nm) and 300 °C (0.84 nm) can be ascribed to the decomposition of the guest L-dopa and partial dehydroxylation of the host layers. When the temperature reached 400 °C, complete decomposition of the interlayer guest and collapse of the layered structure
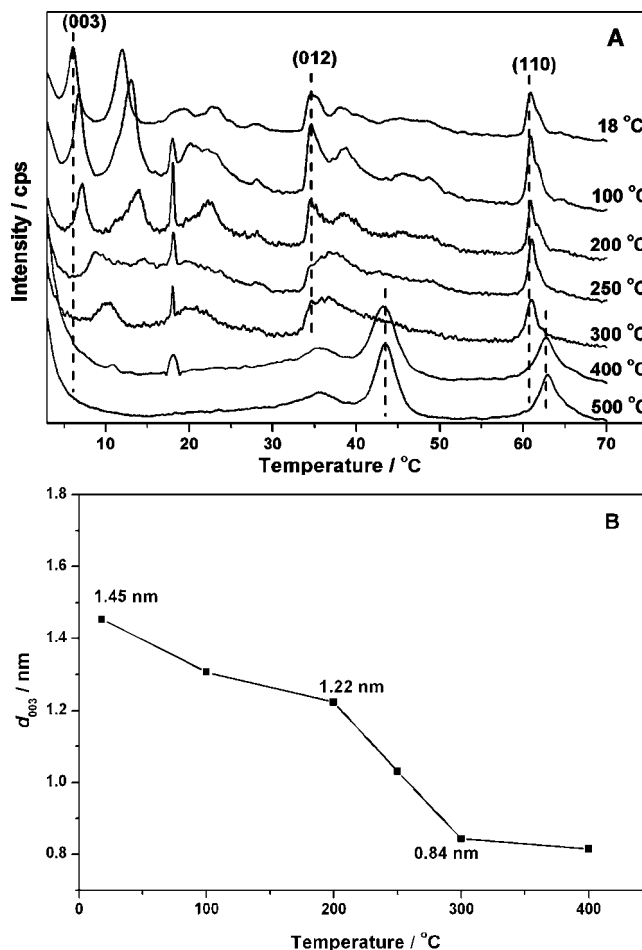

Figure 5. (A) XRD patterns for L-dopa−LDH recorded after heat treatment for 1 h at different temperatures; (B) the relationship between d_{003} basal spacing of L-dopa−LDH and temperature.

occurred, as shown by the disappearance of the characteristic reflections of LDHs and the observation of reflections[10] of MgO at 43.54° and 62.86°.

4.2.2. TG/DTA and TG−MS Analysis of Samples. The TG/DTA curves of pristine L-dopa and L-dopa−LDH are shown in Supporting Information Figure S1. L-Dopa itself (Supporting Information Figure S1a) exhibited two weight loss events above 270 °C. The first sharp event occurred in the temperature range of 270−350 °C (ca. 45 wt %), associated with the melting and decomposition of L-dopa (melting point 295 °C). Correspondingly, a sharp endothermic peak appeared in the DTA curve (Supporting Information Figure S1a′). The second weight loss (450−650 °C) can be attributed to the combustion of L-dopa, and a very broad exothermic peak was observed at 512 °C in the DTA curve (Supporting Information Figure S1a′). In the case of L-dopa−Mg/Al-LDH (Supporting Information Figure S1b), its thermal decomposition was characterized by two weight loss events: one from room temperature to 200 °C (ca. 10 wt %; calcd 9.1%) resulting from the removal of the external surface adsorbed and interlayer water molecules, with a corresponding weak endothermic peak in the DTA curve (Supporting Information Figure S1b′); the other, in the temperature range of 300−550 °C (ca. 35%) being a continuous weight loss process in which the slow weight loss event (300−400 °C) may involve simultaneously partial dehydroxylation of the

Scheme 2. Schematic Representation of the Homolytic Cleavage Processes for (A) L-Dopa and (B) L-Dopa Intercalated LDH
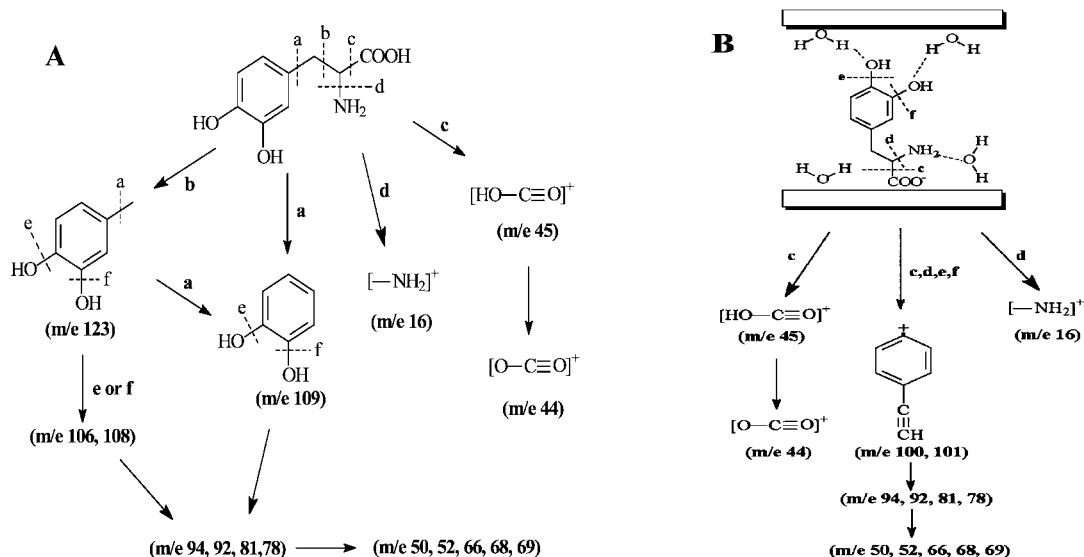

brucite-like layers and decomposition of L-dopa anions, whereas the sharp weight loss (400−550 °C) arises from the combustion of guest anion and complete dehydroxylation of the host layers, with a corresponding strong exothermic peak at 436 °C in the DTA curve (Supporting Information Figure S1b′).

The decomposition behavior of L-dopa and L-dopa−LDH was also studied by TG−MS (Supporting Information Figure S2). Only minor differences were observed in the identity of the fragments detected during decomposition of L-dopa and L-dopa−LDH (Supporting Information Figure S2 and Table S3). In both cases, characteristic signals appeared at $m/e = 16$ (amido), 18 (water), 44−45 (carbon dioxide and carboxyl),[39a] and 50−52, 66−69, 78−81 (fragments resulting from decomposition of the phenyl ring).[39b] Some differences were observed for larger fragments with m/e values over 90, which suggests that the host−guest interactions in L-dopa−LDH may affect the decomposition of L-dopa. A possible interpretation of the observed fragment m/e values is given in Scheme 2. For pristine L-dopa (Scheme 2A), some large fragments can be produced via route a or b, which subsequently give smaller fragments by further decomposition (such as by route e, f, or fragmentation of the benzene ring). In addition, carboxyl (m/e 45), carbon dioxide (m/e 44), and amido (m/e 16), can be directly produced by fragmentation via routes c and d. As for L-dopa intercalated into LDH (Scheme 2B), as a result of the effects of various host−guest interactions including the hydrogen bonding between guest anions, the hydroxyl groups of host layers and interlayer water molecules, homolytic cleavage may initially occur via routes c, d, e, and f, and thus some larger fragments (m/e 100, 101) are formed initially. Smaller fragments, similar to those formed by decomposition of pristine L-dopa, such as m/e 78, 66, 52, 50, etc., were formed when further decomposition occurred. The homolytic cleavage processes of the two samples shown in Scheme 2 are in good agreement with the experimental results.

The evolution of emitted fragments as a function of increasing temperature was also analyzed. In the case of

L-dopa−LDH (Supporting Information Figure S3B), an intense ion peak with m/e 18 was observed below 200 °C, which can be attributed to loss of interlayer water. From 300 to 500 °C, two intense ion peaks with m/e 18 ($[H_2O]^+$) and 44 ($[CO_2]^+$) were simultaneously observed. These can be attributed to dehydroxylation of host layers and decomposition of guest L-dopa anions, in agreement with the TG/DTA results. The evolution of other representative fragments for L-dopa and L-dopa−LDH is also shown in Supporting Information Figure S3, such as peaks with m/e 50, 81, 106, and 123 from L-dopa (Supporting Information Figure S3A) and with m/e 45, 50, 69, 81, and 100 from L-dopa−LDH (Supporting Information Figure S3B). It should be noted that although the fragments from pristine L-dopa were observed between 300 and 450 °C (Supporting Information Figure S3A), the fragments from the L-dopa guest were only detected above 400 °C (Supporting Information Figure S3B), indicating that the thermal stability of L-dopa has been enhanced significantly by intercalation into the LDH host.

4.3. Comparison of the Rates of Racemization of L-Dopa before and after Intercalation into LDHs. The influence of intercalation in the LDH host on the stereochemical stability of L-dopa was investigated. The effects of three factors (sunlight, UV light, and heat treatment) on the optical activity of L-dopa were studied. As shown in Figure 6, the rates of racemization of pristine L-dopa and L-dopa intercalated LDH were dramatically different under each of these conditions. During the first 22 h of exposure to sunlight (Figure 6A), the specific optical activity of L-dopa decreased by 38.8%, whereas the specific optical rotation of the intercalated one decreased by only 5.9%. Furthermore, a similar result was obtained for irradiation by UV light (Figure 6B). The value of the specific optical rotation of pristine L-dopa decreased sharply by 38.1% and then remained constant (ca. −7.1°) up to 96 h or even longer exposure time (curve a). In contrast, there was only very slight decrease (less than 4%) in the specific optical rotation of the L-dopa intercalated in the LDH over the same time
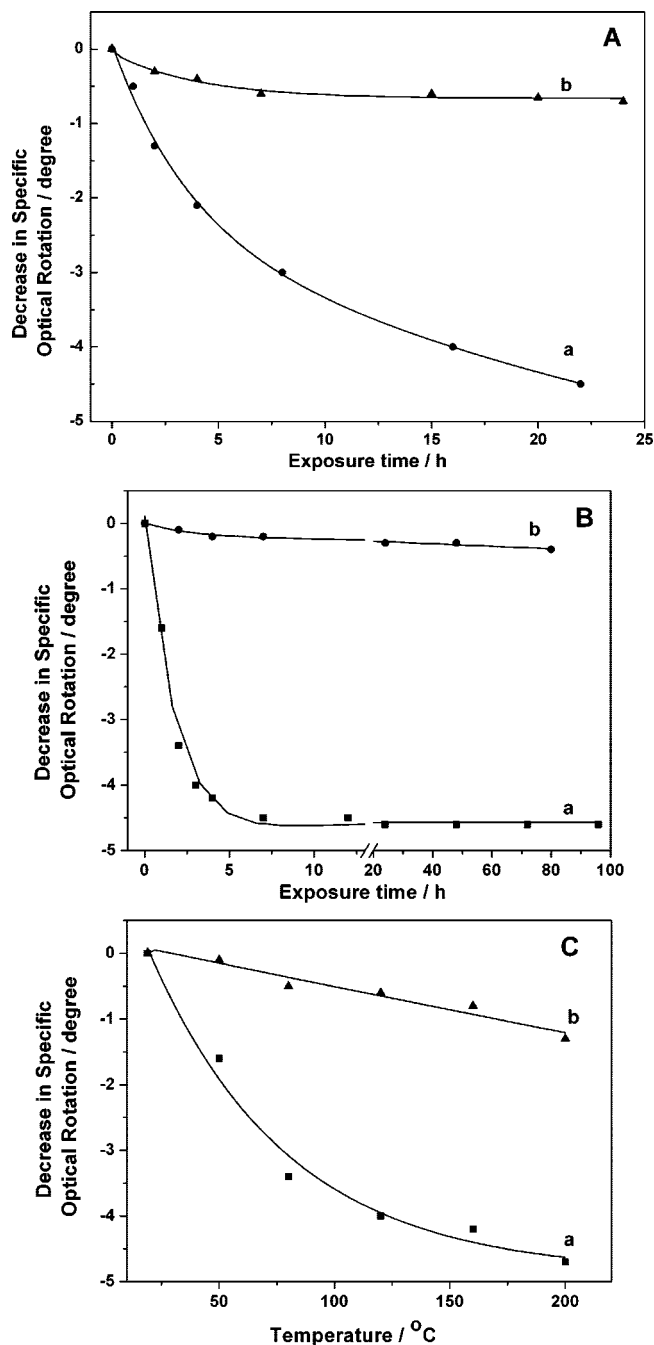
Figure 6. Relationship between the optical activity and (A) the exposure time to sunlight, (B) the exposure time to UV radiation, and (C) the heating temperature for (a) L-dopa and (b) L-dopa−LDH.

under the same conditions (curve b). The influence of temperature on the optical activity of the two samples is illustrated in Figure 6C. The value of specific optical rotation of L-dopa decreased rapidly on increasing temperature, being reduced by 40.5% upon heating at 200 °C (curve a in Figure 6C). However, the value for the intercalated sample decreased by only 11.2% under the same conditions (curve b in Figure 6C).

In order to confirm the reason for the decrease in optical activity of pristine L-dopa, UV−vis and ^{13}C NMR spectra were recorded for the pristine L-dopa exposed to sunlight for 96 h, heated at 200 °C for 1 h, and irradiated by UV light for 22 h. For comparison, the UV−vis and ^{13}C NMR

spectra of fresh L-dopa (without any treatment) were also recorded. In each case, the UV−vis spectra of the samples (Supporting Information Figure S4A) after different treatments were identical to that of the fresh L-dopa, with absorbance maxima at 220.5 and 280.0 nm, consistent with the literature.[40a] Moreover, no significant changes in the ^{13}C spectra (Supporting Information Figure S4B) were observed after the different treatments. Since the chemical structure of L-dopa did not change although the optical activity decreased markedly after the three different treatments, it can be concluded that loss of optical activity was due to racemization of L-dopa rather than its oxidation or other decomposition processes. This racemization process is significantly inhibited when the L-dopa is confined in the interlayer galleries of the LDH.

There have been many studies of the racemization of chiral drugs in solution, both in vitro and in vivo, and the effects of different variables on rate of racemization such as pH of the solution,[41a] solvent effects,[41b] temperature,[41c] and ionic strength,[41d] have also been thoroughly discussed. There have been very few reports of the inhibition of racemization of chiral pharmaceuticals by inclusion in host structures, however. Several workers[42] have investigated the effect of different cyclodextrins (CyDs) (such as α-CyDs, β-CyDs, γ-CyDs and dimethyl-β-CyDs) on racemization and hydrolysis of some chiral drugs and found that the inclusion of the drug in CyDs (with the exception of α-CyDs) can, to some extent, inhibit the attack of hydroxyl ions and/or water molecules and thus retard the racemization and hydrolysis. In our case, the LDHs can be said to act as a "molecular container", providing another effective method for inhibiting racemization of chiral pharmaceuticals.

4.4. Theoretical Study of the Mechanism of Optical Isomerization. *4.4.1. Possible Reaction Mechanism in the Ground State (S₀).* Density functional theory computations have been carried out in order to understand the mechanism of racemization of pristine L-dopa and the reasons for the restricted racemization after intercalation in the LDH host. Although there have been some studies on the mechanism of racemization of amino acids in solution,[43a–c] the mechanism of racemization of chiral molecules in the solid state or in the gas phase has very rarely been studied.[43d] The calculated potential energy profile for the ground state (S₀) of the L-dopa molecule at the B3PW91/6-31G(d,p) level indicates that the minimized energy pathway for racemization involves hydrogen transfer from the chiral carbon atom to carboxyl oxygen via a planar CC⋯H⋯O transition state to give an enol intermediate; then the second hydrogen of the enol group migrates from the carboxyl group to the α-carbon atom via a similar transition state to complete the

(42) (a) Blaschke, G.; Lamparter, E.; Schliiter, J. *Chirality* **1993**, *5*, 78. (b) Bunke, A.; Jira, T.; Beyrich, T. *J. Chromatogr., A* **1996**, *728*, 441. (c) Mey, B.; Paulus, H.; Lamparter, E.; Blaschke, G. *Chirality* **1998**, *10*, 307.
(43) (a) Smith, G. G.; Sivakua, T. *J. Org. Chem.* **1983**, *48*, 627. (b) Swansburg, S.; Buncel, E.; Lemieux, R. P. *J. Am. Chem. Soc.* **2000**, *122*, 6594. (c) Reyes, E.; Córdova, A. *Tetrahedron Lett.* **2005**, *46*, 6605. (d) Sullivan, R.; Pyda, M.; Pak, J.; Wunderlich, B.; Thompson, J. R.; Pagni, R.; Pan, H. J.; Barnes, C.; Schwerdtfeger, P.; Compton, R. *J. Phys. Chem. A* **2003**, *107*, 6674.
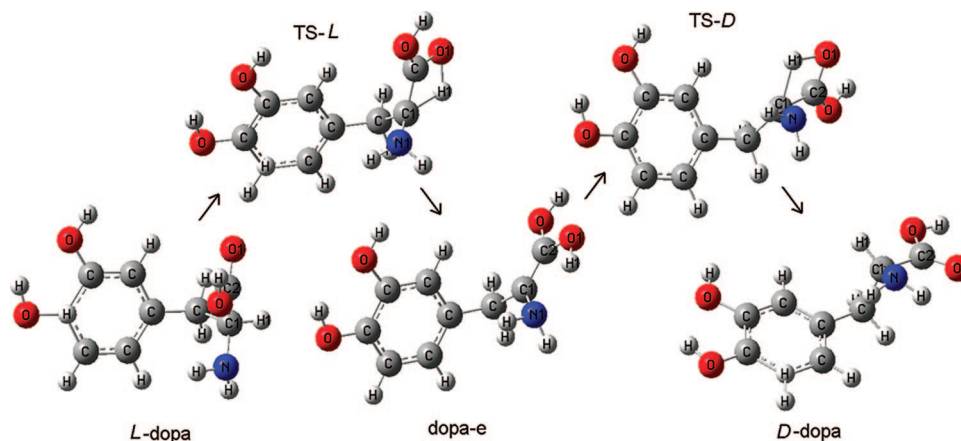
Figure 7. Molecular structures of L-dopa, TS-L, dopa-e, TS-D, and D-dopa in the S_0 state.
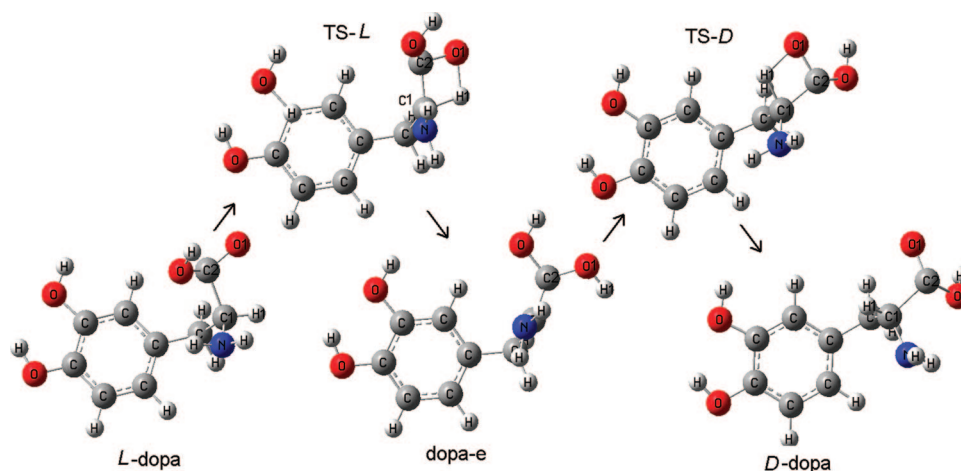
Figure 8. Molecular structures of L-dopa, TS-L, dopa-e, TS-D, and D-dopa in the T_1 state.

racemization process. Figure 7 shows the molecular structures of the reactant (L-dopa), first transition state (TS-L), intermediate (dopa-e), second transition state (TS-D), and product (D-dopa) in the reaction path. The calculated activation energies for the racemization are 303.2 (from L-dopa to dopa-e) and 214.8 kJ/mol (from dopa-e to D-dopa), respectively, indicating that the racemization of L-dopa molecule in the ground state (S_0) may occur only at high temperatures due to the very high energy barrier.

4.4.2. Possible Reaction Mechanism in the Lowest Excited State. The racemization of solid L-dopa molecule also occurs on exposure to UV light, indicating that the reaction may involve the excited state. The computing results of quantum chemistry show that there are also one intermediate of enol form and two transition states in the minimized energy pathway of racemization of L-dopa in the first excited triplet T_1 state. The structural models of the reactant (L-dopa), first transition state (TS-L), intermediate (dopa-e, enol form of dopa), second transition state (TS-D), and product (D-dopa) in the T_1 state shown in Figure 8 are optimized at the level of UB3PW91/6-31 g(d,p) level. Although the corresponding bond lengths of L-dopa, dopa-e, and D-dopa in the S_0 and T_1 state are close, the bond parameters of TS-L and TS-D in the T_1 state differ significantly from those in the S_0 state. Furthermore, the migrating hydrogen atom, the carboxyl carbon, and the carboxyl oxygen are located far from one same plane in the T_1 state. After ZPE correction, the energy

barrier for L-dopa to dopa-e and dopa-e to D-dopa are ca. 55.3 and 113.7 kJ/mol, respectively. Therefore, racemization of L-dopa molecule is feasible in the T_1 state due to the relatively low energy barrier. This agrees well with the experimental phenomenon that the high temperature or UV light can initiate the racemization of L-dopa. In order to inextenso explain the reaction mechanism of the L-dopa molecule, we also calculate the potential energy profiles of the equilibrium state and transition state involved in the reaction in the excited state using TDDFT method at the B3PW91/6-31G(d,p) level. Table 1 lists the critical bond lengths of the reactant, transition states, intermediate, and product in the S_0 and T_1 states, respectively. In order to further verify the transition states of the isomerization path, we calculated the intrinsic reaction coordinate (IRC) at the level of B3PW91/6-31G(d,p). Supporting Information Figures S5 and S6 show the energy curves of S_0 and T_1 states along the IRC path from L-dopa to intermediate and from intermediate to D-dopa. Table 2 gives the energies of different species in the S_0, T_1, and the first excited singlet state (S_1), respectively. The calculations suggest that the L-dopa molecule can be excited to the S_1 state under irradiation by UV light with a wavelength less than 251 nm and subsequently undergo intersystem crossing to the T_1 state. Generally, since the potential energy surfaces of singlet and triplet states are adjacent and the life of the triplet state is relatively long, the intersystem crossing between S_1 and T_1 state is

Table 1. Bond Lengths (nm) of Different Kinds of Species in the S_0 and T_1 States at the B3PW91/6-31G(d,p) Level

	L-dopa		TS-L		dopa-e		TS-D		D-dopa	
	S_0	T_1	S_0	T_1	S_0	T_1	S_0	T_1	S_0	T_1
C1−H1	0.1098	0.1093	0.1537	0.1340	0.2269	0.2553	0.1541	0.1319	0.1097	0.1091
H1−O1	0.2669	0.2373	0.1241	0.1391	0.0985	0.0965	0.1244	0.1397	0.3211	0.2604
C1−N1	0.1449	0.1416	0.1432	0.1377	0.1440	0.1393	0.1451	0.1386	0.1447	0.1410
C2−O1	0.1214	0.1290	0.1296	0.1353	0.1347	0.1396	0.1286	0.1397	0.1210	0.1268

Table 2. Energies (au) of Different Kinds of Species in the S_0, T_1, and S_1 States at the B3PW91/6-31G(d,p) Level

| state	$E_{L\text{-}dopa}$	$E_{TS\text{-}L}$	$E_{dopa\text{-}e}$	$E_{TS\text{-}D}$	$E_{D\text{-}dopa}$
S_0	−704.989765	−704.867969	−704.958973	−704.871608	−704.987381
T_1	−704.840640	−704.815727	−704.864732	−704.818192	−704.846813
S_1	−704.808490	−704.736482	−704.785047	−704.731876	−704.808236

likely to be favorable. The calculated energy barriers for racemization in the T_1 state allow the racemization to take place relatively easily on UV irradiation.

4.4.3. Restriction of LDHs on the Racemization of L-Dopa. The theoretical calculations suggest that in the case of both the thermal and photochemical racemization reactions of L-dopa, the ability of the carboxylate group to act as a hydrogen acceptor and form an enol intermediate is of crucial importance. When L-dopa is intercalated into the interlayer gallery of an LDH, the carboxyl oxygen atoms interact strongly with the hydroxyl hydrogen atoms of the host layers through hydrogen bonding as shown in Figure 9. The computed energies of L-dopa and D-dopa binding to the LDH layers at the B3PW91/6-31G(d,p) level are ca. −1100 kJ/mol. Such a high energy indicates that both L-dopa and D-dopa anions cannot be dissociated into free anions after intercalation into LDHs due to the strong hydrogen bonding. It becomes impossible for the proton attached to the chiral carbon atom of L-dopa or D-dopa to approach the oxygen atom of carboxylate group due to the anchoring interaction between host and guest, so the hydrogen transfer pathway leading to racemization is blocked. Thus, it can be concluded that it is the host−guest interactions between L-dopa and LDH host that inhibit the racemization reaction of the guest.

4.5. In Vitro Drug Release Behavior. It has been reported that in the stomach the pH is 1−2; in the lower part of the small intestine (jejunum and ileum) the pH is maintained at 7.5 ± 0.4, then drops to 6.4 ± 0.6 in the ascending colon, and finally rises again to 7.0 ± 0.7 in the distal colon.[44] The ability of L-dopa−LDHs to act an effective controlled release vehicle for intestinal drug delivery was investigated in a series of in vitro release experiments by monitoring the time dependence of the concentration of L-dopa in simulated intestinal fluids (pH 7.6 and 6.4).

Figure 10 shows the release profiles for the deintercalation of L-dopa from L-dopa−LDH in the two different buffer solutions. In each case, a rapid release during the initial 15 min was followed by a more sustained release of the drug, and 92% and 65% of the total amount of L-dopa was released from the LDH at pH 6.4 and 7.6, respectively. This difference may be explained by reference to the proposed mechanism[28,45] of drug release from such intercalation compounds, which involves an ion-exchange process between guest anions and
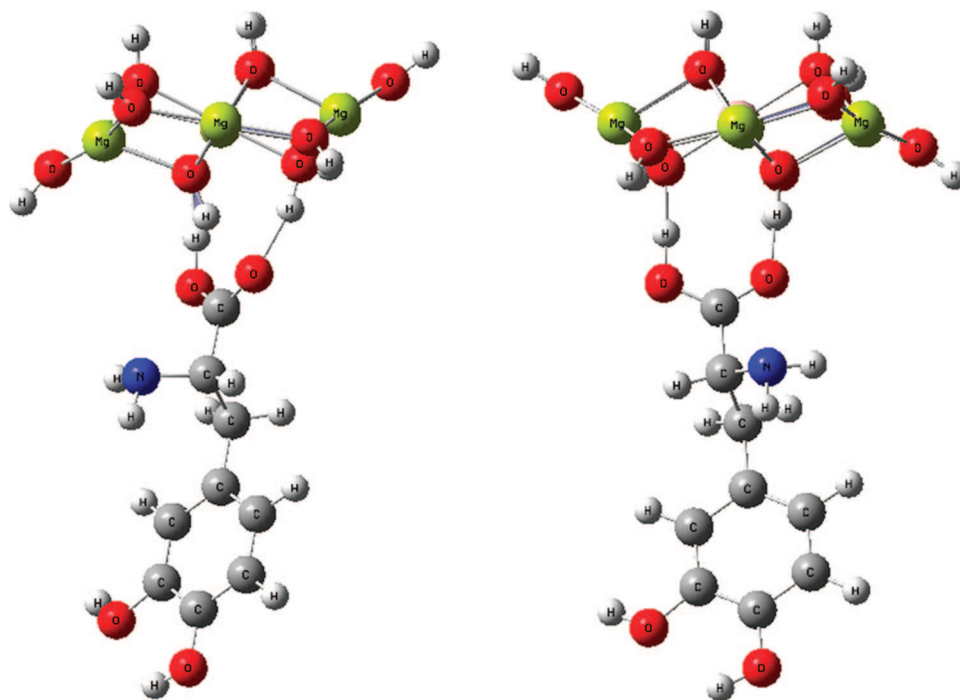
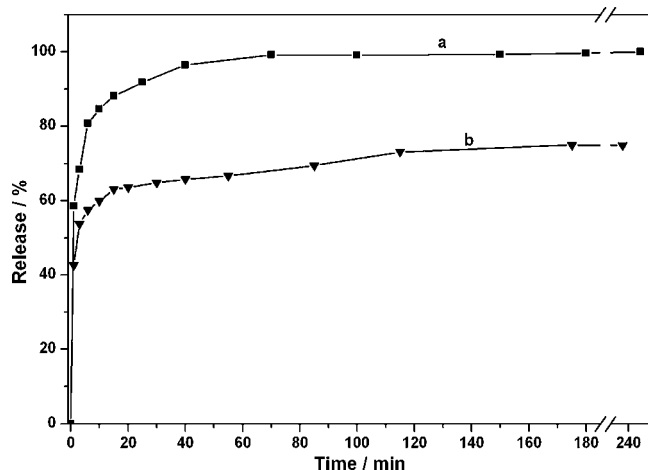**Figure 9.** Schematic representations of L-dopa−LDH (left) and D-dopa−LDH (right).
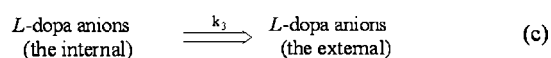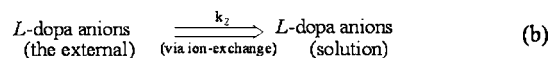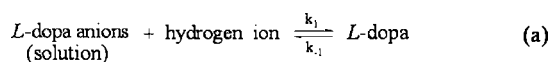
L-*Dopa in Layered Double Hydroxides*

Chem. Mater., Vol. 20, No. 16, 2008 5179

Figure 10. Release profiles of L-dopa from L-dopa–LDH at (a) pH 6.4 and (b) pH 7.6.

Scheme 3. Schematic Representation of the Drug Release Processes of L-Dopa–LDH in a Buffer Solution

$$L\text{-dopa anions (solution)} + \text{hydrogen ion} \underset{k_{-1}}{\overset{k_1}{\rightleftharpoons}} L\text{-dopa} \qquad (a)$$

$$L\text{-dopa anions (the external)} \xrightarrow[\text{(via ion-exchange)}]{k_2} L\text{-dopa anions (solution)} \qquad (b)$$

$$L\text{-dopa anions (the internal)} \xrightarrow{k_3} L\text{-dopa anions (the external)} \qquad (c)$$

phosphate anions contained in the buffer. Boyd et al.[46] reported that in the case of ionic resins, assuming that resin particles are uniform spheres and that sink conditions are maintained, the fraction of drug released is a function of time when the rate-limiting step is the diffusion through the particle. Ambrogi et al.[28b] also carried out kinetic analyses of drug release from LDHs which showed the importance of diffusion through the particle in controlling the drug release rate and reported that the release of ibuprofen depends on the drug concentration (i.e., first-order kinetics), whereas the release of diclofenac depends on the diffusion through the particle. Hence, the following mechanism may be proposed for release of L-dopa from L-dopa–LDHs:

(1)   Diffusion through the solution surrounding the LDH particle: the ionization equilibrium (Scheme 3a) and diffusion of L-dopa anions and phosphate anions in solution (not shown here).

(2)   Reaction in the external parts of the particle: L-dopa anions exchange with the phosphate anions of the medium (Scheme 3b).

(3)   Diffusion through the LDH particle: L-dopa anions diffuse from the internal parts of the LDH particle to the external parts (Scheme 3c).

The rate of exchange of drug anions between the LDH and the solution medium will ultimately be determined by the slowest of these processes. During the first 15 min, the ion exchange probably involves process 2 (Scheme 3b),

accounting for the rapid drug release observed in Figure 10. After L-dopa anions at the edges of the particle are replaced by smaller phosphate anions, diffusion through the particle (Scheme 3c) becomes the rate-determining step, due to the decrease in the interlayer distance,[28] accounting for the subsequent slower release period. The larger amount of drug released at lower pH can be attributed to the higher concentration of hydrogen ions at lower pH which decreases the concentration of L-dopa anions in solution (process 1, Scheme 3a), thus favoring process 2 (Scheme 3b). Similar results have been obtained by other workers in studies of the release of other drugs from LDHs.[47]

5. Conclusions

L-Dopa–Mg/Al-LDH, a host–guest supramolecular hybrid material, was obtained via two successive ion-exchange processes from the nitrate form of the LDH under nitrogen atmosphere and avoiding sunlight. It is proposed that the guest anions are accommodated in the interlayer region as a monolayer through host–guest interactions including electrostatic and hydrogen bonding. UV–vis, FT-IR, and ^{13}C NMR spectroscopy and measurement of the specific optical activity all indicate that both the chemical and stereochemical properties of L-dopa do not change during intercalation in the LDH host.

TG/DTA curves reveal that the decomposition temperature of the intercalated L-dopa increased by 80–100 °C compared with that of the pristine material, and the TG–MS analysis gives a detailed understanding of the homolytic cleavage processes occurring in the two samples. In addition to the increase in thermal stability of L-dopa, its resistance to racemization was also significantly enhanced by intercalation in the LDH host. Computational results using the DFT method at the B3PW91/6-31G(d,p) level suggest that in the solid state L-dopa undergoes racemization via an enol intermediate formed by hydrogen transfer from the chiral carbon atom to the carboxylate group. The racemization energy barrier in the ground S_0 state is 303 kJ/mol and is significantly lower (114 kJ/mol) in the first excited triplet state T_1 state formed by UV-light irradiation. After intercalation in the interlayer galleries of the LDH, the carboxylate group of the L-dopa becomes involved in strong host–guest interactions with the layers, with the computed binding energy of L-dopa to the LDH layers being ca. −1100 kJ/mol. The host–guest interactions, including electrostatic and hydrogen bonding between L-dopa and LDH host, thus inhibit the racemization reaction of the guest because the carboxylate group is no longer able to act as a hydrogen acceptor.

In vitro drug release experiments show that the L-dopa–LDH exhibits controlled release behavior at pH 6.4 and 7.6. Therefore, a combination of experimental measurements and theoretical computations in this work demonstrates that Mg/Al-LDHs are an effective inorganic host material for both inhibition of the racemization of chiral substances during storage prior to application and for controlled delivery at the required time.

(44) Li, B. X.; He, J.; Evans, D. G.; Duan, X. *Int. J. Pharm.* **2004**, *287*, 89.

(45) Wang, Z. L.; Wang, E.; Gao, L.; Xu, L. *J. Solid State Chem.* **2005**, *178*, 736.

(46) Boyd, G. E.; Adamson, A. W.; Myers, L. S., Jr *J. Am. Chem. Soc.* **1947**, *69*, 2836.

(47) Costantino, U.; Casciola, M.; Massinelli, L.; Nocchetti, M.; Vivani, R. *Solid State Ionics* **1997**, *97*, 203.

Supporting Information Available: The values of specific optical rotation of L-dopa (Table S1), the values of pK_a and distribution coefficient δ of L-dopa under the synthesis conditions (Table S2), fragmentation of L-dopa and L-dopa–LDH (Table S3), TG and DTA curves for L-dopa and L-dopa–LDH (Figure S1), 3D scan spectra of TG–MS for L-dopa and L-dopa–LDH (Figure S2), multiple ion detection (MID) spectra of TG–MS for L-dopa and L-dopa–LDH (Figure S3), UV–vis spectra and ^{13}C NMR spectra for L-dopa, L-dopa exposed to sunlight for 96 h, L-dopa irradiated by UV light for 22 h, and L-dopa heated at 200 °C for 1 h (Figure S4), and the IRC energy curves from L-dopa to enol and from enol to D-dopa in the S_0 state (Figure S5) and in the T_1 state (Figure S6) (PDF). This material is available free of charge via the Internet at http://pubs.acs.org.

CM800035K